Title

The role of Rydberg and continuum levels in computing high harmonic generation spectra of the hydrogen atom using time-dependent configuration interaction

Journal

The Journal of Chemical Physics, 139(16)

ISSN

0021-9606

Authors

Luppi, Eleonora
Head-Gordon, Martin

Publication Date

2013-10-28

DOI

10.1063/1.4824482

Peer reviewed

The role of Rydberg and continuum levels in computing high harmonic generation spectra of the hydrogen atom using time-dependent configuration interaction

Eleonora Luppi

Laboratoire de Chimie Théorique, Université Pierre et Marie Curie, 75005 Paris, France

Martin Head-Gordon

Department of Chemistry, University of California Berkeley,

and Chemical Sciences Division, Lawrence Berkeley

National Laboratory, Berkeley CA 94720, USA.

(Dated: September 23, 2013)

Abstract

We study the role of Rydberg bound-states and continuum levels in the field-induced electronic dynamics associated with the High-Harmonic Generation (HHG) spectroscopy of the hydrogen atom. Time-dependent configuration-interaction (TD-CI) is used with very large atomic orbital expansions (up to $L = 4$ with sextuple augmentation and off-center functions) to describe the bound Rydberg levels, and some continuum levels. To address the lack of ionization losses in TD-CI with finite AO basis sets, we employed a heuristic lifetime for energy levels above the ionization potential. The heuristic lifetime model is compared against the conventional atomic orbital treatment (infinite lifetimes), and a third approximation which is TD-CI using only the bound levels (continuum lifetimes go to zero). The results suggest that spectra calculated using conventional TD-CI do not converge with increasing AO basis set size, whilst the zero lifetime and heuristic lifetime models converge to qualitatively similar spectra, with implications for how best to apply bound state electronic structure methods to simulate HHG. The origin of HHG spectral features including the cutoff and extent of interference between peaks is uncovered by separating field-induced coupling between different types of levels (ground state, bound Rydberg levels, and continuum) in the simulated electronic dynamics. Thus the origin of deviations between the predictions of the semi-classical three step model and the full simulation can be associated with particular physical contributions, which helps to explain both the successes and the limitations of the three step model.

I. INTRODUCTION

The study of atomic and molecular processes in intense ultrashort laser fields is a subject of increasing interest since the advent of attosecond (10^{-18} s) laser pulse generation, characterization and application [1–8]. In fact, the recent impressive advances in laser technology are continuously triggering the introduction of new spectroscopic and measurement methods, which offer the opportunity to investigate unexplored research areas in atoms and molecules with unprecedented time resolution [7–12].

Attosecond pulses may be obtained via the high-harmonic generation (HHG) process, which can provide coherent XUV and soft X-ray radiation with a sub-femtosecond temporal resolution. HHG is a highly nonlinear phenomenon [13], where the optical spectrum has a distinctive shape: a rapid decrease for the low-order harmonics consistent with perturbation theory, followed by a broad plateau region where the harmonic intensity drops more slowly, and then an abrupt cutoff, beyond which no harmonics are observed. Associated with these characteristics is the fact that the harmonic emission spectrum is composed of coherent radiation lines with equally spaced frequencies.

The HHG process can be understood by semiclassical models [14, 15] where three important assumptions are made: (i) an electron escapes from the nuclei through tunnel ionization associated with the strong laser field, and (ii) it is accelerated away by the laser field until the sign of the field changes, (iii) whereupon the electron is reaccelerated back to the Coulomb field of the nuclei, where it may emit a photon (a harmonic of the laser field) as it returns towards the ground state. It is possible to roughly estimate when these assumptions are valid through the Keldysh parameter (γ) which describes the balance between the amount of energy carried by the laser field and the energy which is necessary for an electron to escape to the continuum. γ is defined[16] as $\gamma = \sqrt{I_p/(2U_p)}$ where I_p is the ionization potential and $U_p = E_0^2/(4\omega_0^2)$ is the ponderomotive energy (E_0 is the laser amplitude and ω_0 is the carrier frequency of the laser field). If $\gamma > 1$ we are in the the multiphoton regime, while if $\gamma < 1$ we are in the tunneling regime. From this simple model it is also possible to obtain the position of the cutoff in the HHG spectrum, associated with the maximum energy the field can impart to the electron, which is $E_{\text{cutoff}} = I_p + 3.17U_p$. Most previous theoretical descriptions employ approaches where it is assumed that only a single electron is "active" [17–20], consistent with the semi-classical three step model reviewed above. However, even

if these semiclassical models have explained some key features of the HHG spectra, the true electronic dynamics is more complicated and the importance of quantum mechanical properties of the many-electron dynamics in strong laser field has been pointed out [21, 22].

When the laser interacts with the system a non-stationary electronic wave-packet is generated, consisting of a coherent superposition of excited states. Time-evolution of the wave-packet corresponds to the dynamics, and involves changing interference between the different excited states in the wave-packet. The wave-packet and its dynamics are strongly determined by parameters of the laser such as intensity, duration, polarization and phase of carrier frequency.

The proper treatment of this many-electron dynamics under the influence of the laser field is obtained by solving the time-dependent Schrödinger equation which is only possible in very limited cases, even with semi-classical treatment of the molecule-field interaction. For an approximate solution, time-dependent density-functional theory (TDDFT) [23–27] is widely employed. Recently, wavefunction based methods have been extended to the time-domain. Examples include multiconfigurational time-dependent Hartree-Fock (MCTDHF) [28–34], a direct method to solve the time-dependent coupled-cluster equations [35] and time-dependent configuration-interaction [36–45] using singly excited states (TD-CIS) with perturbative (TD-CIS(D)) and full (TD-CISD) corrections for double excitations. Recently, we used the last class of time-dependent wavefunction method and we found that they are also quite valuable for predicting HHG in small molecular systems [45].

In this paper, we discuss in detail the role of the Rydberg bound-states and the continuum levels for the time-dependent dynamics responsible for HHG in the model case of the H atom [17, 46] using time-dependent configuration-interaction (TD-CI) in an atomic orbital (AO) expansion. The first issue is what are the implications of using a finite AO basis set? With a finite AO basis, ionization losses do not occur, because the electron never fully escapes the atom. What consequences does this have for convergence of the results as the AO basis is improved to better describe the bound Rydberg levels and the continuum? Grid-based methods typically employ a complex absorbing potential (CAP) or other method ("mask function") to capture outgoing waves associated with ionization [47]. In the AO description, one can associate a heuristic lifetime with energy levels above the ionization potential [42] to approximately achieve the same result. This model correctly allows an electron that has been excited to very high energy states because of the acceleration imposed by the field to

escape (be absorbed) with high probability such that it does not contributes to the HHG. We shall compare the heuristic model (finite lifetimes for nonstationary levels), which is appropriate for high-field problems, against the conventional AO treatment which assumes infinite lifetimes, and a third approximation which is to assume the lifetimes go to zero (effectively removing the continuum levels entirely). These results have implications for the manner in which bound state electronic structure methods are best applied to simulate HHG.

With the overall form of the HHG spectrum under control, the second issue that we consider is the origin of the spectral features including the cutoff and the extent of interference between peaks in terms of the electronic dynamics. Contributions from field-induced coupling between different types of levels can be separated in the simulation in order to deduce their effects on the observed HHG spectrum. Thus the origin of deviations between the predictions of the semi-classical three step model of the full simulation can be associated with particular physical contributions. For example, we can separate the role of field-induced coupling between different excited bound levels (i.e. the Rydberg series) from the coupling between the ground state and the Rydberg levels, as well as coupling to the continuum levels. These results help to explain both the successes and the limitations of the three step model. The remainder of the paper consists of a description of the overall time-dependent quantum approach, as well as simulation details, followed by a presentation of the results.

II. THEORY

We consider the case of the H atom in an external laser field. The time-dependent Schrödinger equation (TDSE) (atomic units $e^2 = \hbar = m = 1$) is

$$i\frac{\partial\Psi(\mathbf{r},t)}{\partial t} = \left(-\frac{\nabla^2}{2} - \frac{1}{|\mathbf{r}|} - \hat{\mathbf{r}}\cdot\mathbf{F}(t)\right)\Psi(\mathbf{r},t), \tag{1}$$

where $-\hat{\mathbf{r}}\cdot\mathbf{F}(t)$ represents the interaction between the H atom and the time-dependent external laser field $\mathbf{F}(t)$ in the semiclassical dipole approximation. The electric field $\mathbf{F}(t)$ is represented as

$$\mathbf{F}(t) = \mathbf{n}f(t)sin(\omega_0 t + \phi) \tag{2}$$

where $\mathbf{n}$ is a unit vector in the direction of the (linear) electric field polarization, $f(t)$ is the envelope function, ω_0 is the carrier frequency and ϕ is the phase. In this article, we employ

a cos^2 shape for the envelope function

$$f(t) = \begin{cases} f_0 cos^2(\frac{\pi}{2\sigma}(\sigma - t)) & \text{if } |t-\sigma| \leq \sigma, \\ 0 & \text{otherwise.} \end{cases}$$

where σ is the width of the field envelope.

We represent $\Psi(\mathbf{r}, t)$ using time-dependent configuration interaction (TD-CI) where $\Psi(\mathbf{r}, t)$ is expanded in a truncated eigenstate basis composed of the ground state ($|\psi_0\rangle$), and time-independent (field free) CI excited states, ($|\psi_k\rangle, k > 0$):

$$|\Psi(t)\rangle = \sum_{k=0} \tilde{R}_k(t)|\psi_k\rangle. \tag{3}$$

In applying this many-electron methodology to our specific case of the H atom, considering a given basis set of size K we obtain 1 occupied molecular orbital $|\phi_1\rangle$ and $v = K-1$ virtual orbitals $|\phi_a\rangle$. $|\psi_0\rangle = |\phi_1\rangle$ while the excited states are single orbital substitutions. $|\psi_a\rangle = |\phi_a\rangle$ For the H atom, the field-free CI matrix is trivially diagonal, although the same methodology can applied to many-electron systems where different configurations do interact to yield the field-free eigenstate basis. For details of the time-(in)dependent CI equations we refer the reader to existing reviews [48].

Inserting the time-dependent wavefunction, Eq. (3), into Eq. (1) and projecting with bras corresponding to the HF ground state and the CI excited states, we obtain a time-dependent equation for the coefficients:

$$i\frac{d\tilde{R}_k(t)}{dt} = \sum_s (E_k^{CI}\delta_{ks} - \boldsymbol{r}_{ks} \cdot \mathbf{F}(t))\tilde{R}_s(t), \tag{4}$$

where the initial condition at $t = 0$ is chosen to be the ground state represented in the chosen basis.

In order to solve this equation we approximate the time integral by discretizing the time of the propagation and we make use of a split propagator technique as the Hamiltonian is the sum of two independent terms: the field-free hamiltonian and the laser field in the dipole approximation. With these two assumptions we can write the solution of the time-dependent propagation in TD-CI in matrix notation as

$$\tilde{\mathbf{R}}(t + \Delta t) = \mathbf{U}^\dagger e^{i\boldsymbol{r}\cdot\mathbf{F}(t)\Delta t}\mathbf{U}e^{-i\mathbf{E}^{CI}\Delta t}\tilde{\mathbf{R}}(t) \tag{5}$$

The matrix $\mathbf{E}^{CI}$ is the diagonal matrix of the field-free hamiltonian in the basis of the CI eigenstates, while the matrix $\boldsymbol{r} \cdot \mathbf{F}(t)$ describes the dipole-field interaction. The matrix $\mathbf{U}$

is the unitary matrix describing the change of basis between the CI eigenstate basis, and a basis in which the dipole-field interaction is diagonal. Once the time-dependent coefficients are known also the time-dependent wavefunction, $\Psi(\mathbf{r},t)$, is known, making possible to monitor the time-dependent dynamics of the electrons through the induced dipole-moment $\boldsymbol{\mu}(t) = \langle\Psi(\mathbf{r},t)|\hat{\boldsymbol{\mu}}|\Psi(\mathbf{r},t)\rangle$ which is calculated as

$$\boldsymbol{\mu}(t) = \sum_{s,k} \tilde{R}_s^*(t)\tilde{R}_k(t)\boldsymbol{\mu}_{sk}, \tag{6}$$

where $\boldsymbol{\mu}_{sk} = \langle\psi_s|\hat{\boldsymbol{\mu}}|\psi_k\rangle$. The power spectrum of the HHG is then acquired by taking the Fourier transform of the total time-dependent induced dipole moment, $\boldsymbol{\mu}(t)$

$$P(\omega) = \left|\frac{1}{t_f - t_i}\int_{t_i}^{t_f} \boldsymbol{\mu}(t)e^{-i\omega t}dt\right|^2. \tag{7}$$

HHG is in competition with ionization processes which cannot be modeled directly by TD-CI, due to the lack of continuum basis functions (we assume that TD-CI employs finite atomic orbital basis expansions, as used in bound state electronic structure codes). For the same reason, contributions to the electron dynamics of HHG from the continuum are also not properly treated by TD-CI. Analogous problems exist in grid-based wavepacket propagation, and are dealt with by approaches such as a CAP [37, 49], complex scaling [50, 51], or a wavefunction absorber [47]. We shall use the recent heuristic model proposed by Klinkusch et al. [42] to describe laser-induced electron dynamics including photoionization with TD-CI in AO basis sets. This model allows for the treatment of ionizing states as nonstationary states with a finite, energy-dependent lifetime to account for above-threshold ionization losses in laser-driven many-electron dynamics. The CI eigenstates ($\mathbf{E}^{CI}$) with energies above the ionization threshold are interpreted as non-stationary and replaced with complex energies:

$$\mathbf{E}^{CI} \rightarrow \mathbf{E}^{CI} - \frac{i}{2}\boldsymbol{\Gamma}, \tag{8}$$

$\boldsymbol{\Gamma}$ is a diagonal matrix where $\Gamma_{nm} = \Gamma_n\delta_{nm}$ and Γ_n is the ionization rate of CI energy state n, which is related to the lifetime of that state as $\tau_n = 1/\Gamma_n$. The heuristic model was developed for (time-dependent) configuration-interaction with single substitutions((TD)-CIS), which rely on prior solution of the Hartree-Fock equations for the field-free system. The resulting ground-state Slater determinant of occupied molecular orbitals, $|\phi_i\rangle$, is written as $|\psi_0^{HF}\rangle = ||\phi_1\rangle|\phi_2\rangle...|\phi_l\rangle|$ where $l = N/2$ (N is the number of electrons). Considering a given basis set

of size K we obtain l occupied molecular orbitals $|\phi_i\rangle$ and $\nu = K - l$ virtual orbitals $|\phi_a\rangle$. The CIS wavefunction for the state $n > 0$ is defined as

$$|\Psi_n^{CIS}\rangle = \sum_{ia} C_{i,n}^a |\Psi_i^a\rangle. \tag{9}$$

$|\Psi_i^a\rangle$ are singly excited determinants where an electron was excited from the occupied orbital $|\phi_a\rangle$ to the virtual orbital $|\phi_r\rangle$. In the case of one electron, the (TD-)CIS become an exact (TD-)CI with $C_{1,n}^a = \delta_{an}$. To obtain the ionization rate, Klinkusch et al. [42] considered that an electron in a virtual orbital a with energy $\epsilon_a > 0$ has the classical kinetic energy $\epsilon_a = \frac{1}{2}v^2$ where v is the escape velocity of the electron, which is defined as $v = \frac{d}{\tau}$. Here d is a parameter that is the characteristic escape length which the electron can travel during the time interval, τ, which is the lifetime (or inverse of the ionization rate, $\tau = \Gamma^{-1}$) of the one-electron system, so that $\Gamma = \sqrt{2\epsilon_r}/d$. Based on these considerations, the ionization rate of the CIS state n is given by:

$$\Gamma_n = \begin{cases} 0 \text{ if } \mathbf{E}_n^{CI} < I_p, \\ \sum_{ia} |C_{i,n}^a|^2 \sqrt{2\epsilon_a}/d \text{ if } \mathbf{E}_n^{CI} > I_p \quad \text{and} \quad \epsilon_a > 0 \end{cases}$$

This model is appropriate for the high field case where above-threshold ionization is dominant, and is similar to a complex absorbing potential in energy space [42].

III. RESULTS

In TD-CI, the time-dependent wave function is expanded using a finite number of field-free electronic states and dipole moments from a corresponding static CI calculation. We took these matrix elements from calculations using the Q-Chem software package [52], and employed in a small external program we have written to propagate the time-dependent wave-packet. These methods all employ finite Gaussian atomic orbital basis expansions.

All HHG spectra presented in this article were computed for a cos^2-shaped laser field (see Eq.(2)) with carrier frequency ω_0= 1.55 eV (corresponding to a Ti:sapphire laser) and a duration of the pulse that is 20 optical cycles (o.c.) (σ = 10 o.c.), where 1 o.c = $2\pi/\omega_0$. The polarization of the field was chosen to be linear and parallel to the $\hat{\mathbf{z}}$ direction. The TD-CI calculations were propagated using a time step of 0.24 as (0.01 au) for a total duration of 40 o.c. The simulations reported in this paper used an intensity of I=10^{14} W/cm^2, which was tested against I=10^{13} W/cm^2 and I=10^{15} W/cm^2.

In order to have a good representations of the bound excited states comprising the Rydberg series, we used augmented Dunning quintuple-zeta basis. Whilst up to double augmentation is common [53–55] (corresponding to adding two extra shells of each angular momentum), this will only adequately describe the $n = 2$ states. Therefore we also included from 3 up to 6 sets of diffuse shells, defining the t-aug-cc-pV5Z, through s-aug-cc-pV5Z basis sets. The sextuply augmented basis thus consists of 11s,10p,9d,8f,7g shells, for a total of 205 functions. To ensure numerical stability with this largest basis, we had to remove the two most diffuse g functions, leaving a basis comprised of 11s,10p,9d,8f,5g shells, for a total of 187 functions.

The Rydberg energies calculated with this sequence of basis sets are shown in Fig. (1). It is evident that as more diffuse functions are included in the AO basis, more excited Rydberg states are correctly reproduced. In particular, with the s-aug-cc-pv5z basis we can fully describe the (Rydberg) bound states through $n = 5$: $n = 1$ ($E = -0.500$, 1 state), $n = 2$ ($E = -0.125$, 4 states), $n = 3$ ($E = -0.055$, 9 states), $n = 4$ ($E = -0.031$, 16 states), $n = 5$ ($E = -0.020$, 25 states). In addition this basis provides an incomplete description of $n = 6$ ($E = -0.014$, 16 of 36 states) and $n = 7$ ($E = -0.010$, 1 of 49 states), as well as a very partial (and poor) description of some continuum (unbound levels).

To achieve some further representation of the unbound continuum levels, we also constructed two "super" basis sets that enhance the s-aug-cc-pv5z basis with six ghosts atoms arranged octahedrally on a sphere of radius 1 a.u. These ghost functions are either cc-pVDZ or cc-pVTZ on each of the 6 sites. The "super-DZ" basis has 217 basis functions in total, whilst the "super-TZ" basis has 271 basis functions in total. The CI continuum energy-states are shown in Fig. (2). The total number of CI states obtained is 186 for s-aug-cc-pV5Z, 216 for s-aug-cc-pV5Z plus six cc-pVDZ ghost atoms, and 270 for s-aug-cc-pV5Z plus six cc-pVTZ ghost atoms.

HHG spectra from TD-CI with the 3 different basis sets, s-aug-cc-pV5Z, s-aug-cc-pV5Z plus six cc-pVDZ ghost atoms, and s-aug-cc-pV5Z plus six cc-pVTZ ghost atoms, are shown in Fig. 3. The curves show peaks at the odd harmonics with decreasing intensities as the order increases. Based on the 3 step model [14, 15], we expect to observe a cutoff around the 21st harmonic. However, the calculated spectra shows signal up to about the 25th harmonic. However because of strong interference effects, it is difficult to distinguish structure and signal in the HHG spectra from the background.

Fig. 3 shows a large background signal is present in these HHG spectra calculated with finite basis TD-CI . For the intensity used (I=10^{14} W/cm^2), the background is similar for all three calculations, however we observed for higher intensities that the background increases as the basis set is enlarged, and therefore as the number of localized unbound states included in the calculation is increased. In fact it is expected that calculated HHG spectra cannot be feasibly converged to a limiting form as the finite basis is enlarged. Energy levels above the ionization potential correspond to an electron that is no longer bound to the nucleus. Therefore amplitude in such levels may well lead to ionization in the HHG dynamics, rather than reforming the neutral atom. However, as the unbound states are localized in finite AO basis TD-CI, no such ionization channel is open, and they can contribute to the HHG spectrum. Adding more and more localized yet unbound levels to the TD-CI therefore will not give convergent spectra until the spatial extent of the AO's is sufficient so that outgoing flux is not reflected on the timescale of the simulation.

The non-convergent behavior of the calculated TD-CI HHG spectra can be corrected by allowing for the possibility of ionization, by applying the heuristic model to give an energy-dependent lifetime to all energy levels above the ionization potential I_p. In this way the CI eigenstates with energies above the ionization threshold are interpreted as non-stationary, and possible ionization from high-energy levels is accounted for. As can be seen in Fig. 4, adding a lifetime to the unbound states appears to solve the problem of artifactual contributions to HHG from high-energy levels. In particular, with finite lifetimes, the calculated spectra appear to be satisfactorily convergent as the AO basis is improved to s-aug-cc-pV5Z plus six cc-pVTZ ghost atoms. Evidently removal of spurious recombination and interference effects from the quantum dynamics also removes most of the basis set-dependent background signal in the HHG spectra calculated without lifetimes, as follows from comparing Fig. 3 and Fig. 4. In order to apply the heuristic lifetime model we had to choose a value for the escape length. We started by considering that the maximum radial extension of the electron is equal to $\frac{E_0}{\omega^2}$ following the three step model. Considering our laser parameter we obtain $16.6a_0$. Therefore, we tested our calculations using $d = 16.6a_0$, and also the smaller value $d = 1.4a_0$ and a larger value of $d = 100a_0$. We found that the results are not strongly affected by the choice of the escape length and for the calculations reported here, we used $d = 1.4a_0$.

It is interesting to compare the HHG spectra computed this way against other methods

that properly treat the continuum [17]. For instance, Bandrauk et al. [17] calculated HHG spectra from numerical solution of the Schrödinger equation for the hydrogen atom interacting with a linearly polarized laser pulse. They used the same parameters for the laser as we used, except that the carrier envelope has a Gaussian form and was propagated for a slightly shorter time. Directly comparing our HHG spectrum with theirs, we find quite good agreement. We observe that our harmonic peaks are sharper then theirs, which presents some more complex structures. Moreover, in our case we also observe that the background is higher and it appears to partly obscure the harmonic signal. The overall structure of the signal is not much affected by the heuristic lifetimes, suggesting that ground and bound excited states are primarily responsible for the HHG. We note that we both have a plateau region around -8 (on a $\log_{10}$ scale). The background in our case starts around -12.5 while in their case it starts lower at around -14.

As the other limiting case, we also computed HHG with TD-CI after completely removing the continuum states (all the field-free states above I_p, as shown in 2) before propagation (zero lifetime). As is evident in Fig. 5, the spectra obtained this way are in reasonable agreement with the heuristic model using finite lifetimes. The overall intensity is slightly higher and the peaks show slightly more structure. As a practical matter, this result suggests that a reasonable approach to using bound-state codes for HHG spectral simulations is to simply delete the continuum states. This result also shows that there is an important role for the (bound) Rydberg excited states in the HHG electron dynamics.

Given the reasonable predictions of the HHG spectrum using the heuristic (finite) lifetime model, we next report investigations on the electronic dynamics exploiting the ease of separating the different contributions included in the TD-CI wavefunction (Eq. (3)) and in the propagation equation (Eq. (4)). We shall use the following abbreviations for the different contributions: ground (G), bound (B) and continuum (C). We can develop Eq. (3) as

$$|\Psi(t)\rangle = G(t)|\psi_0\rangle + \sum_{b=1}^{N_b} B_b(t)|\psi_b\rangle + \sum_{c=1}^{N_c} C_c(t)|\psi_c\rangle, \tag{10}$$

where N_b is the number of bound excited states and N_c is the number of continuum states associated with a chosen basis set. The same type of separation can also be performed for the energy and the dipole matrices appearing in Eq. (4) for the calculation of the time-dependent coefficients of the wavefunction.

The terms describing interference between G, B and C can be explicitly identified. All

the matrices have dimension $K \times K$ where $K = 1 + N_b + N_c$ and have the following general form in terms of G, B and C

$$\begin{pmatrix} G\text{-}G & G\text{-}B & G\text{-}C \\ B\text{-}G & B\text{-}B & B\text{-}C \\ C\text{-}G & C\text{-}B & C\text{-}C \end{pmatrix}.$$

Here $G-G$ is a 1×1 matrix describing the interaction of the ground state with itself, $G-B$ ($B-G$) is a vector of dimension $1 \times N_b$ ($N_b \times 1$) describing the interaction of ground-bound (bound-ground) states and $G-C$ ($C-G$) is also a vector of dimension $1 \times N_c$ ($N_c \times 1$) describing the interaction of ground-continuum (continuum-ground) states. Finally, $B-B$ is a matrix of dimension $N_b \times N_b$ and $C-C$ of dimension $N_c \times N_c$ describing respectively the bound-bound and continuum-continuum interactions.

The total time-dependent dipole (and as a consequence HHG) can also be written in terms of G, B and C time-dependent dipole contributions by expanding the time-dependent expectation value:

$$\begin{aligned} \boldsymbol{\mu}(t) = \; & \boldsymbol{\mu}_{GG}(t) \; + \boldsymbol{\mu}_{GB,BG}(t) + \boldsymbol{\mu}_{GC,CG}(t) + \boldsymbol{\mu}_{BB}(t) + \\ & \boldsymbol{\mu}_{BC,CB}(t) + \boldsymbol{\mu}_{CC}(t), \end{aligned} \tag{11}$$

where

$$\boldsymbol{\mu}_{GG}(t) = G^*(t)G(t)\boldsymbol{\mu}_{0,0}, \tag{12}$$

$$\boldsymbol{\mu}_{GB,BG}(t) = \sum_{b=1}^{N_b} (G^*(t)B_b(t)\boldsymbol{\mu}_{0,b} + B_b^*(t)G(t)\boldsymbol{\mu}_{b,0}), \tag{13}$$

$$\boldsymbol{\mu}_{GC,CG}(t) = \sum_{c=N_b+1}^{N_c} (G^*(t)C_c(t)\boldsymbol{\mu}_{0,c} + C_c^*(t)G(t)\boldsymbol{\mu}_{c,0}), \tag{14}$$

$$\boldsymbol{\mu}_{BB}(t) = \sum_{b=1}^{N_b} \sum_{b\prime=1}^{N_b} B_b^*(t)B_{b\prime}(t)\boldsymbol{\mu}_{b,b\prime} \tag{15}$$

$$\boldsymbol{\mu}_{BC,CB}(t) = \sum_{b=1}^{N_b} \sum_{c=N_b+1}^{N_c} (B_b^*(t)C_c(t)\boldsymbol{\mu}_{b,c} + C_c^*(t)B_b(t)\boldsymbol{\mu}_{c,b}) \tag{16}$$

$$\boldsymbol{\mu}_{CC}(t) = \sum_{c=N_b+1}^{N_c} \sum_{c\prime=N_b+1}^{N_c} C_c^*(t)C_c(t)\boldsymbol{\mu}_{c,c\prime}. \tag{17}$$

The HHG spectra shown in Fig. (3) and Fig. (4) are obtained from a time-dependent propagation where G, B and C contributions describe the time-dependent effects such as

ground- and excited-state depletion, ionization, and recombination. This gives us the physical information about the elaborate role of every electronic state in the HHG and in principle allows us to identify the energy transfer among harmonics, laser field and the electrons in the HHG process. Therefore, we shall henceforth regard the full time-dependent propagation with heuristic lifetimes as our "benchmark" solution, and now proceed to characterize the electronic dynamics that is primarily responsible for the HHG signal.

A first approach to this task is to start from the "benchmark" solution for the TD-CI wave function, and then include only particular partial contributions to the time-dependent dipole moment and thus the power spectrum. In this approach, the time-dependent coefficients appearing in the partial dipoles still conserve all the information about the full time-dependent propagation, i.e. all possible interferences between G, B and C. In Fig. 6 we compare HHG as obtained from the total time-dependent dipole (Eq. 11) (full propagation) and from the partial time-dependent dipoles (Eqs (12,13,14,15,16,17)).

All the spectra in Fig. 6 have a very similar shape and it is mainly the intensity that changes. We observe that in the region where there is a clear harmonic signal, the $G-C$, $G-B$ and BB have almost the same intensity as the full propagation, while in the background region the larger contributions primarily originate from the $B-B$ terms. However, because the time-dependent coefficients still conserve the full propagation information, it is clear that these contributions cancel each other to a large extent when summed to give the full result. This indicates that the partial contributions cannot be expected to yield much physical information individually.

In order analyze HHG on the basis of G, B and C contributions avoiding cancellation effects, we turned to a second approach in which we also modified the Hamiltonian of the propagation. First, we started by setting the $B-B$ perturbation to zero in Eq. (4) which reduces to

$$\begin{pmatrix} G\text{-}G & G\text{-}B & G\text{-}C \\ B\text{-}G & 0 & B\text{-}C \\ C\text{-}G & C\text{-}B & C\text{-}C \end{pmatrix}.$$

This also means that $\boldsymbol{\mu}_{BB}$ is equal to zero in the time-dependent dipole moment (Eq. 15) .

Second, we also set to zero all the other possible contributions from B states:

$$\begin{pmatrix} G\text{-}G & 0 & G\text{-}C \\ 0 & 0 & 0 \\ C\text{-}G & 0 & C\text{-}C \end{pmatrix},$$

which makes $\boldsymbol{\mu}_{GB,BG}$, $\boldsymbol{\mu}_{BC,CB}$ equal to zero in the time-dependent dipole moment (Eqs. 13,16). Third, the $C-C$ perturbation was also set to zero

$$\begin{pmatrix} G\text{-}G & 0 & G\text{-}C \\ 0 & 0 & 0 \\ C\text{-}G & 0 & 0 \end{pmatrix},$$

making $\boldsymbol{\mu}_{CC}$ equal to zero in the time-dependent dipole moment (Eq. 17). In this last case we obtain a propagation which is very similar to the physical mechanism of the 3SM as we do not include any transitions between bound states and interactions/recombinations between continuum and bound states. Note that in all these three cases we do not lose any cancellation effects as it is straightforward to observe that the time-dependent dipole is coherent with the Hamiltonian propagation.

In Fig. (7) HHG spectra calculated in the three ways described above are compared with a full propagation. First, it is interesting to see that neglecting the BB contribution effectively removes the background in the HHG spectrum, which makes possible to discover a number of harmonics that were previously below the background level. The magnitude of the background depends very strongly on the presence of the bound states and is primarily determined by the bound-bound interactions. We confirm similar earlier findings [47] where the sensitivity of the background to the number of bound states was also deduced.

Comparing the HHG where we neglected BB coupling to those where all bound states were removed, we observe that the bound states contribute to the higher part of the spectra close to the cutoff region. We also observed that these two parts of the spectrum (the cutoff region and the background) are strongly modulated by the intensity of the laser we used in the simulation. In fact, as in these regions the main contributions come from the bound states, increasing or decreasing the laser intensity changes the depletion of the ground states, the extent of excitation into the Rydberg states and the ionization in the continuum. In other words, the intensity changes affect how Rydberg bound states can interfere.

The blue HHG curve presented in Fig. 7 was calculated considering only the interaction between the ground and continuum states. We started from an Hamiltonian which is able to describe the physical mechanism ascribed to the 3SM model: ionization, propagation in the laser field and recombination of the returning electronic wave packet with the ground-state. Continuing to take as a reference the cutoff from 3SM, we see that our simulation reveals that the HHG signal ends at much lower harmonics than the predicted cutoff. However, the first and more intense harmonics are evidently due to the mechanism described by the 3SM. We conclude that even if the 3SM seems to give reasonable results, the harmonics appear to be the overall result of several mechanisms, depending very much on the bound states in question [56]. In fact, the lowest harmonics are well described by all the simplified models, while harmonics close to the cutoff region, and the background, strongly depend on the interference of the bound excited states with the ground state, themselves, and the continuum.

To go deeper towards understanding the role of the Rydberg bound states we calculated the HHG neglecting the bound-bound contributions as a function of the principal quantum number, n, as shown in Fig. 8. We started by considering only $n = 1$ (G contribution) and $n = 2$ ($E = -0.125$, 4 states). Then we progressively included higher Rydberg states: first $n = 3$ ($E = -0.055$, 9 states), then $n = 4$ ($E = -0.03125$, 16 states), $n = 5$ ($E = -0.020$, 25 states) and $n = 6$ ($E = -0.014$, 16 states). The lowest harmonics are well described by $n = 1, 2$, however the inclusion of higher Rydberg levels creates distinct plateaus at different energy ranges related to the Rydberg states in question.

This effect clarifies the role of the Rydberg states in developing new methods to extend the plateau of the harmonic generation to higher energies. For example, by preparing the initial state as a coherent superposition of the ground state and an excited state it is possible to induce dipole transitions between the continuum and the ground state via the intermediate bound(excited)-state. This new scheme may provide a way of controlling the coherent output that is produced in an experiment [57–59].

Moreover, this means that if a smaller basis with fewer diffuse functions is used such as d-aug-cc-pV5Z, t-aug-cc-pV5Z, q-aug-cc-pV5Z, p-aug-cc-pV5Z, etc, we obtain roughly the same trend observed in Fig. 8 because of the varying number of Rydberg bound-states that can be correctly described by the different basis sets.

The results presented here illustrate the roles of G, B and C states in HHG dynamics.

Whilst we have only reported results for a single set of field parameters, the same qualitative results are found for a range of parameters of the laser field. However, we observed that TD-CI with heuristic lifetimes is not able to describe HHG as the laser intensity increases towards around I=10^{15} W/cm^2. In this regime, the ionization processes start to compete strongly with HHG, and limitations of the heuristic lifetime model become evident. Only the first harmonics are reproduced while the rest of the spectrum is an undistinguishable mix of background and harmonics due to the artifacts of the interference between G, B and C. With an intense field such as I=10^{15} W/cm^2, most of the dynamics is played by the high continuum levels, which because of the heuristic model, also have relatively large lifetimes. This has the consequence that most of the electron dynamics is lost. By decreasing the heuristic lifetimes, it is possible to obtain slightly better behavior. However, this also makes new structure coming from spurious interactions appear in the HHG dynamics. Most sophisticated approaches such as the complex scaling method [30, 50] are probably necessary in this regime.

IV. CONCLUSIONS

In this work, we have presented a detailed study of the role of Rydberg bound-states and continuum in High-Harmonic Generation (HHG) Spectroscopy using time-dependent configuration-interaction for the H atom. We improved the atomic orbital basis to better describe the bound Rydberg levels and the continuum levels. We explicitly demonstrated that a full propagation with bound state code including all levels does not converge with AO basis set and gives artifacts in the form of an increasingly strong background. The basic problem is that ionization losses do not occur in finite atomic orbital basis, because the electron never fully escapes the atom.

To address this issue, we employed a heuristic lifetime model [42] for energy levels above the ionization potential, to approximately allow an electron that has been excited to very high energy states to escape and not contribute to the HHG. We compared the heuristic model (finite lifetimes for non-stationary levels) against the conventional atomic orbital treatment which assumes infinite lifetimes, and a third approximation which is to assume the lifetimes go to zero (effectively removing the continuum levels entirely). These results have implications for the manner in which bound state electronic structure methods are best

applied to simulate HHG. The use of heuristic lifetime model gives HHG spectra that converge with basis set and are in reasonable agreement with other methods that properly treat the continuum as long as the laser intensity is not too high (10^{14} W/cm^2). Removing the continuum states entirely (zero lifetimes) gives an HHG spectrum in reasonable agreement with the heuristic model (slightly higher intensities). This appears to be the preferable way to use a bound state code without the heuristic lifetimes.

We also considered the origin of the HHG spectral features including the cutoff and the extent of interference between peaks in terms of the electronic dynamics. Contributions from field-induced coupling between different types of levels can be separated in the simulation in order to deduce their effects on the observed HHG spectrum. Thus the origin of deviations between the predictions of the semi-classical three step model, and the full simulation can be associated with particular physical contributions. We can separate the role of field-induced coupling between different excited bound levels (i.e. the Rydberg series) from the coupling between the ground state and the Rydberg levels, as well as coupling to the continuum levels. Considerably insight into the success and limitation of the semiclassical 3 step model can be obtained by selectively removing coupling between different types of levels in the simulations. The origin of the HHG cutoff is more complicated than implied by the 3 step model. These results help to explain both the successes and the limitations of the three step model.

V. ACKNOWLEDGEMENTS

Funding for this research has been provided by the Department of Energy through the USXL program at Lawrence Berkeley National Laboratory. We acknowledge computational resources obtained under NSF award CHE-1048789.

[1] P. M. Paul, E. S. Toma, P. Breger, G. Mullot, F. Augé, P. Balcou, H. G. Muller, and P. Agostini, Science **292**, 1689 (2001).

[2] M. Hentschel, R. Kienberger, C. Spielmann, G. A. Reider, N. Milosevic, T. Brabec, P. Corkum, U. Heinzmann, M. Drescher, and F. Krausz, Nature (London) **414**, 509 (2001).

[3] F. Quéré, Nature Phys. **5**, 93 (2009).

[4] O. Smirnova and M. Ivanov, Nature Phys. **6**, 159 (2010).

[5] S. Baker, I. A. Walmsley, J. W. G. Tisch, and J. P. Marangos, Nature Phys. **5**, 664 (2011).

[6] G. Sansone, L. Poletto, and M. Nisoli, Nature Phys. **5**, 655 (2011).

[7] P. B. Corkum and F. Krausz, Nature Phys. **3**, 381 (2007).

[8] F. Krausz and M. Ivanov, Rev. Mod. Phys. **81**, 163 (2009).

[9] J. Itatani, J. Levesque, D. Zeidler, H. Niikura, H. Ppin, J. C. Kieffer, P. B. Corkum, and D. M. Villeneuve, Nature (London) **432**, 867 (2004).

[10] E. Goulielmakis, Z.-H. Loh, A. Wirth, R. Santra, N. Rohringer, V. S. Yakovlev, S. Zherebtsov, T. Pfeifer, A. M. Azzeer, M. F. Kling, S. R. Leone, and F. Krausz, Nature (London) **466**, 739 (2010).

[11] S. Haessler, J. Caillat, W. Boutu, C. Giovanetti-Teixeira, T. Ruchon, T. Auguste, Z. Diveki, P. Breger, A. Maquet, B. Carré, R. Taïeb, and P. Salières, Nature Phys. **6**, 200 (2010).

[12] G. Sansone, F. Kelkensberg, J. F. Pérez-Torres, F. Morales, M. F. Kling, W. Siu, O. Ghafur, P. Johnsson, M. Swoboda, E. Benedetti, F. Ferrari, F. Lépine, J. L. Sanz-Vicario, S. Zherebtsov, I. Znakovskaya, A. L'Huillier, M. Y. Ivanov, M. Nisoli, F. Martín, and M. J. J. Vrakking, Nature **465**, 763 (2010).

[13] P. Antoine, A. L'Huillier, and M. Lewenstein, Phys. Rev. Lett. **77**, 1234 (1996).

[14] P. B. Corkum, Phys. Rev. Lett. **71**, 1994 (1993).

[15] M. Lewenstein, P. Balcou, M. Y. Ivanov, A. LHuillier, and P. B. Corkum, Phys. Rev. A **49**, 2117 (1994).

[16] L. V. Keldysh, Sov. Phys. JETP, **20**, 1307 (1965).

[17] A. Bandrauk, S. Chelkowski, D. Diestler, J. Manz, and K. J. Yuan, Phys. Rev. A **79**, 023403 (2009).

[18] A. Gordon, F. Kärtner, N. Rohringer, and R. Santra, Phys. Rev. Lett. **96**, 223902 (2006).

[19] R. Taïeb, V. Véniard, J. Wassaf, and A. Maquet, Phys. Rev. A **68**, 033403 (2003).

[20] C. Ruiz, L. Plaja, R. Taïeb, V. Véniard, and A. Maquet, Phys. Rev. A **73**, 063411 (2006).

[21] N. Nguyen and A. Bandrauk, Phys. Rev. A **73**, 032708 (2006).

[22] S. Patchkovskii, Z. Zhao, T. Brabec, and D. M. Villeneuve, Phys. Rev. Lett. **97**, 123003 (2006).

[23] M. E. Casida, Time-dependent density functional response theory for molecules, in *Recent Advances in Density Functional Methods*, edited by D. P. Chong, Part I, page 155, World

Scientific, Singapore, 1995.

[24] J. F. Dobson, Time-dependent density functional theory, in *Electronic Density Functional Theory : Reccent Progress and New Directions*, edited by J. F. Dobson, G. Vignale, and M. P. Das, Plenum Publishing Corporation, New York, 1997.

[25] E. Runge and E. K. U. Gross, Phys. Rev. Lett. **52**, 997 (1984).

[26] E. K. U. Gross and W. Kohn, Phys. Rev. Lett. **55**, 2850 (1985).

[27] A. Castro, M. A. L. Marques, and A. Rubio, J. Chem. Phys. **121**, 3425 (2004).

[28] J. Caillat, J. Zanghellini, M. Kitzler, O. Koch, W. Kreuzer, and A. Scrinzi, Phys. Rev. A **71**, 012712 (2005).

[29] M. Nest, R. Padmanaban, and P. Saalfrank, J. Chem. Phys. **126**, 214106 (2007).

[30] D. Haxton, K. Lawler, and C. McCurdy, Phys. Rev. A **83**, 063416 (2011).

[31] F. Remacle and R. Levine, Phys. Rev. A **83**, 013411 (2011).

[32] F. Remacle, M. Nest, and R. Levine, Phys. Rev. Lett. **99**, 183902 (2007).

[33] P. Redkin and R. Ganeev, Phys. Rev. A **81**, 063825 (2010).

[34] C. Jhala and M. Lein, Phys. Rev. A **81**, 063421 (2010).

[35] C. Huber and T. Klamroth, J. Chem. Phys. **134**, 054113 (2011).

[36] N. Rohringer, A. Gordon, and R. Santra, Phys. Rev. A **74**, 043420 (2006).

[37] L. Greenman, P. Ho, S. Pabst, E. Kamarchik, D. Mazziotti, and R. Santra, Phys. Rev. A **82** (2010).

[38] P. Krause, T. Klamroth, and P. Saalfrank, J. Chem. Phys. **123**, 074105 (2005).

[39] P. Krause, T. Klamroth, and P. Saalfrank, J. Chem. Phys. **127**, 034107 (2007).

[40] H. B. Schlegel, S. M. Smith, and X. Li, J. Chem. Phys. **126**, 244110 (2007).

[41] G. Floß, T. Klamroth, and P. Saalfrank, Phys. Rev. B **83**, 104301 (2011).

[42] S. Klinkusch, P. Saalfrank, and T. Klamroth, J. Chem. Phys. **131**, 114304 (2009).

[43] J. A. Sonk, M. Caricato, and H. B. Schlegel, J. Phys. Chem. A **115**, 4678 (2011).

[44] J. A. Sonk and H. B. Schlegel, J. Phys. Chem. A **115**, 11832 (2011).

[45] E. Luppi and M. Head-Gordon, Molecular Physics **110**, 909 (2012).

[46] G. Bandarage, A. Maquet, T. Ménis, R. Taïeb, V. Véniard, and J. Cooper, Physical Review A **46**, 380 (1992).

[47] J. L. Krause, K. J. Schafer, and K. C. Kulander, Phys. Rev. A **45**, 4998 (1992).

[48] A. Dreuw and M. Head-Gordon, Chem. Rev. **105**, 4009 (2005).

[49] R. Santra and L. S. Cederbaum, The Journal of Chemical Physics **117**, 5511 (2002).

[50] N. Moiseyev, Physics Reports **302**, 212 (1998).

[51] W. P. Reinhardt, Annu. Rev. Phys. Chem. **82**, 223 (1982).

[52] Y. Shao, L. F. Molnar, Y. Jung, J. Kussmann, C. Ochsenfeld, S. T. Brown, A. T. B. Gilbert, L. V. Slipchenko, S. V. Levchenko, D. P. O Neill, R. A. DiStasio Jr, R. C. Lochan, T. Wang, G. J. O. Beran, N. A. Besley, J. M. Herbert, C. Yeh Lin, T. Van Voorhis, S. Hung Chien, A. Sodt, R. P. Steele, V. A. Rassolov, P. E. Maslen, P. P. Korambath, R. D. Adamson, B. Austin, J. Baker, E. F. C. Byrd, H. Dachsel, R. J. Doerksen, A. Dreuw, B. D. Dunietz, A. D. Dutoi, T. R. Furlani, S. R. Gwaltney, A. Heyden, S. Hirata, C.-P. Hsu, G. Kedziora, R. Z. Khalliulin, P. Klunzinger, A. M. Lee, M. S. Lee, W. Liang, I. Lotan, N. Nair, B. Peters, E. I. Proynov, P. A. Pieniazek, Y. Min Rhee, J. Ritchie, E. Rosta, C. David Sherrill, A. C. Simmonett, J. E. Subotnik, H. Lee Woodcock III, W. Zhang, A. T. Bell, A. K. Chakraborty, D. M. Chipman, F. J. Keil, A. Warshel, W. J. Hehre, H. F. Schaefer III, J. Kong, A. I. Krylov, P. M. W. Gill, and M. Head-Gordon, Physical Chemistry Chemical Physics **8**, 3172 (2006).

[53] R. Kendall, T. Dunning, and R. Harrison, J. Chem. Phys. **96**, 6796 (1992).

[54] D. Woon and T. Dunning, J. Chem. Phys. **98**, 1358 (1993).

[55] D. Woon and T. Dunning, J. Chem. Phys. **100**, 2975 (1994).

[56] C. F. de Morisson Faria, M. Dörr, and W. Sandner, Physical Review A **58**, 2990 (1998).

[57] J. B. Watson, A. Sanpera, X. Chen, and K. Burnett, Physical Review A **53**, 1962 (1996).

[58] Z. Zhai, Q. Zhu, J. Chen, Z.-C. Yan, P. Fu, and B. Wang, Physical Review A **83**, 043409 (2011).

[59] A. Sanpera, J. B. Watson, M. Lewenstein, and K. Burnett, Physical Review A **54**, 4320 (1996).

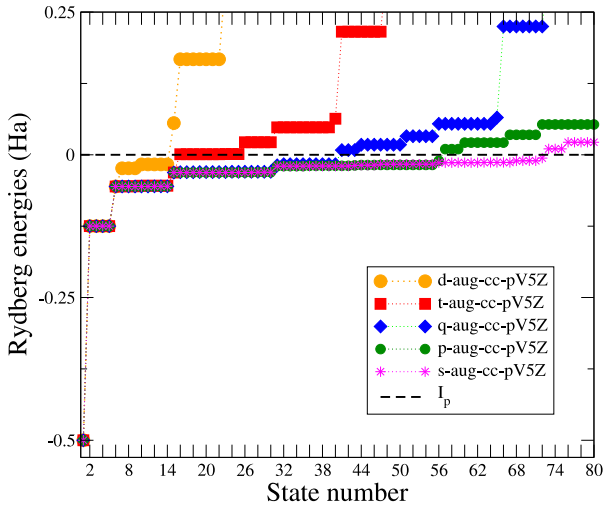

FIG. 1. Rydberg bound state energies for the d-aug-cc-pV5Z, t-aug-cc-pV5Z, q-aug-cc-pV5Z, p-aug-cc-pV5Z and s-aug-cc-pV5Z basis sets.

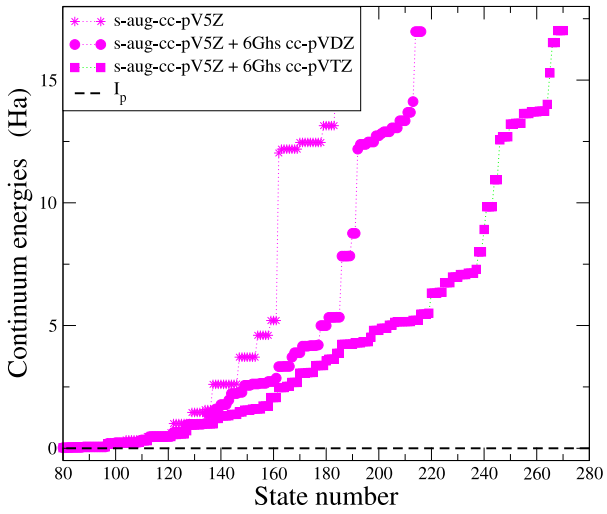

FIG. 2. Unbound continuum levels obtained with the s-aug-cc-pV5Z, s-aug-cc-pV5Z plus six cc-pVDZ ghost atoms, and s-aug-cc-pV5Z plus six cc-pVTZ ghost atoms.

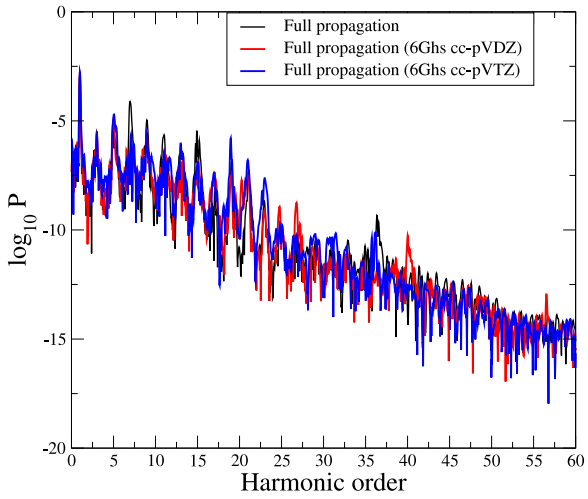

FIG. 3. HHG spectra from full propagation calculations using s-aug-cc-pV5Z, s-aug-cc-pV5Z plus six cc-pVDZ ghost atoms, and s-aug-cc-pV5Z plus six cc-pVTZ ghost atoms.

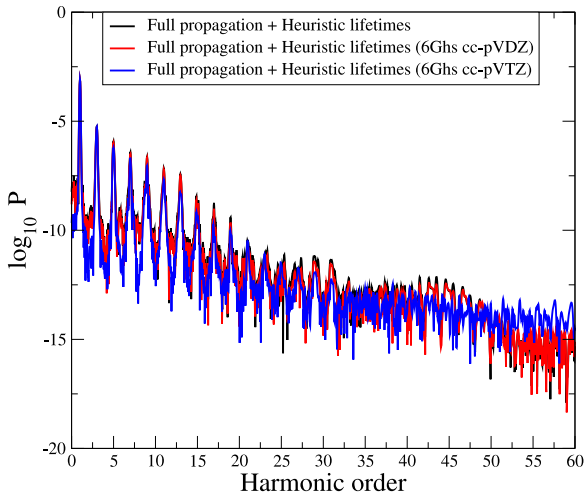

FIG. 4. HHG spectra from full propagation calculations with finite lifetimes for unbound states, using s-aug-cc-pV5Z, s-aug-cc-pV5Z plus six cc-pVDZ ghost atoms, and s-aug-cc-pV5Z plus six cc-pVTZ ghost atoms.

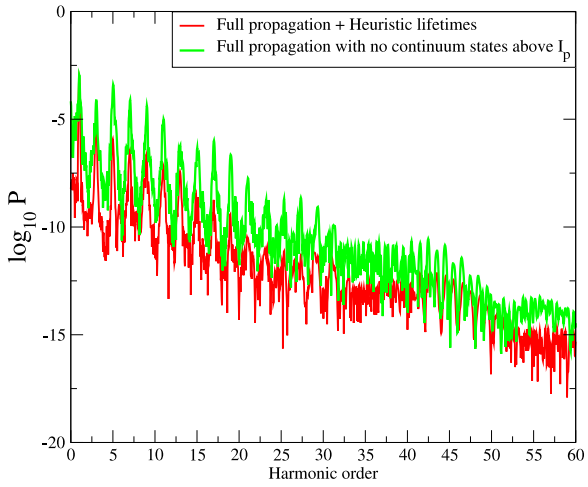

FIG. 5. HHG spectra from a TD-CI propagation calculation where the continuum was treated by using the heuristic lifetime model (red trace) or completely removed (green trace).

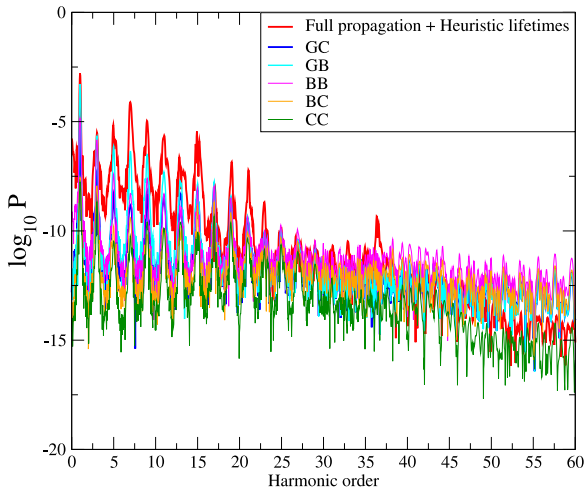

FIG. 6. Comparison between HHG spectrum from full propagation with lifetimes with HHG spectra with lifetimes from GC, GB, BB, BC and CC partial contributions.

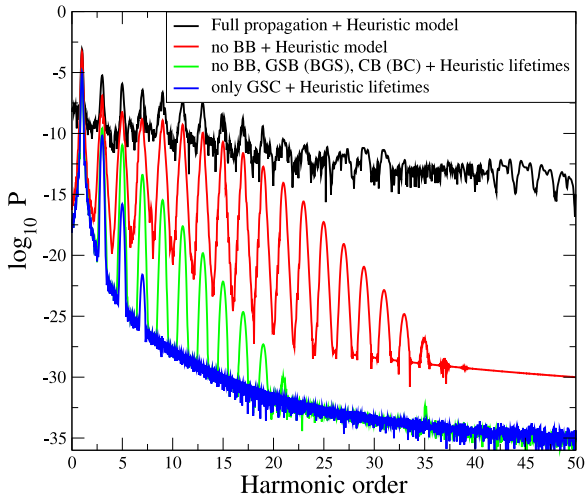

FIG. 7. HHG spectra from full propagation (black), without BB contribution (red), without BB, GB (BG) and CB (BC) contributions (green) and only with GC (CG) contributions (blue). All spectra have been calculated using heuristic lifetimes for unbound levels and with the s-aug-cc-pV5Z basis set.

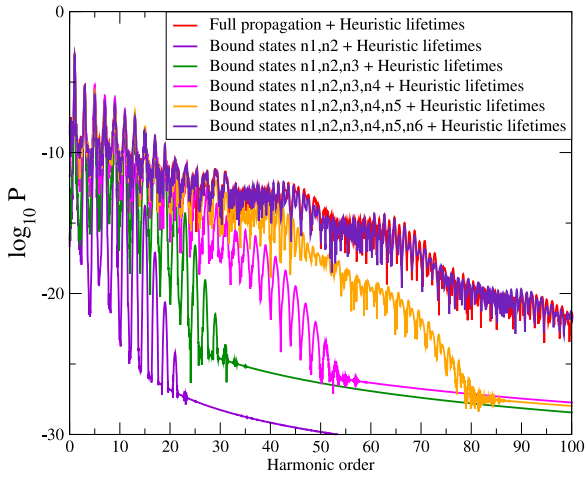

FIG. 8. Assessing the role of the Rydberg bound states in HHG by systematically neglecting bound-bound contributions to the dynamics as a function of the shell n. The basis s-aug-cc-pV5Z was used.